

PCCP

Accepted Manuscript



This is an *Accepted Manuscript*, which has been through the Royal Society of Chemistry peer review process and has been accepted for publication.

Accepted Manuscripts are published online shortly after acceptance, before technical editing, formatting and proof reading. Using this free service, authors can make their results available to the community, in citable form, before we publish the edited article. We will replace this *Accepted Manuscript* with the edited and formatted *Advance Article* as soon as it is available.

You can find more information about *Accepted Manuscripts* in the [Information for Authors](#).

Please note that technical editing may introduce minor changes to the text and/or graphics, which may alter content. The journal's standard [Terms & Conditions](#) and the [Ethical guidelines](#) still apply. In no event shall the Royal Society of Chemistry be held responsible for any errors or omissions in this *Accepted Manuscript* or any consequences arising from the use of any information it contains.

Metal-Organic Kagome Lattices, $M_3(2, 3, 6, 7, 10, 11\text{-hexaiminotriphenylene})_2$ ($M = \text{Ni}$ and Cu): From Semiconducting to Metallic by Metal Substitution

Cite this: DOI: 10.1039/x0xx00000x

Shuang Chen, Jun Dai and Xiao Cheng Zeng*

Received 00th January 2012,

Accepted 00th January 2012

DOI: 10.1039/x0xx00000x

www.rsc.org/

Motivated by recent experimental synthesis of a semiconducting metal-organic graphene analogue (*J. Am. Chem. Soc.* 2014, **136**, 8859), *i.e.*, $\text{Ni}_3(2, 3, 6, 7, 10, 11\text{-hexaiminotriphenylene})_2$ [$\text{Ni}_3(\text{HITP})_2$], a new Kagome lattice, $\text{Cu}_3(\text{HITP})_2$, is designed by substituting the coordination of Ni by Cu. Such substitution results in interesting changes in electronic properties of $M_3(\text{HITP})_2$ bulk and two-dimensional (2D) sheets. In $\text{Ni}_3(\text{HITP})_2$, each Ni atom adopts the dsp^2 hybridization, forming a perfect 2D conjugation, whereas in $\text{Cu}_3(\text{HITP})_2$, each Cu atom adopts the sp^3 hybridization, resulting in a distorted 2D sheet. The $M_3(\text{HITP})_2$ bulks, assembled from $M_3(\text{HITP})_2$ sheets via both strong π - π interaction and weak metal-metal interaction, are metallic. However, the 2D $\text{Ni}_3(\text{HITP})_2$ sheet is semiconducting with a narrow band gap whereas the 2D $\text{Cu}_3(\text{HITP})_2$ sheet is metallic. Remarkably, both the 2D $M_3(\text{HITP})_2$ Kagome lattices possess Dirac bands in the vicinity of the Fermi level. Additional *ab initio* molecular dynamics simulations show that both sheets exhibit high thermal stability at elevated temperatures. Our theoretical study offer new insights into tunability of electronic properties for the 2D metal-organic frameworks (MOFs).

Introduction

Two-dimensional (2D) functional materials, including graphene,¹ graphene derivatives,² layered metal chalcogenides,³ and 2D covalent-organic frameworks (COFs),^{4, 5} have attracted intensive attention owing to their novel electronic, optical, and mechanical properties for future device applications. Graphene, a single layer of sp^2 -bonded carbon atoms in a honeycomb lattice, is a 2D carbon allotrope. However, the lack of a bandgap limits its device application.⁶ The graphene derivatives possess a bandgap but at the expense of decreased charge carrier mobility.⁷ Two new classes of 2D materials, transition metal chalcogenides⁷⁻¹⁰ and COFs,^{11, 12} are also viewed as potential alternatives to graphene derivatives since the transition metal chalcogenides can be easily produced in large area with controlled thicknesses¹³ while the organic COFs can be chemically modified.¹¹ However, the chemical functionalization of metal chalcogenides is difficult and the carrier mobility of COFs tends to be depressed due to the reduction of in-plane conjugation resulting from COF's own flexibility or the presence of functional groups in the building blocks. A new class of metal-organic frameworks (MOFs) assembled from square-planar metal ions and aromatic organic moieties, such as *o*-semiquinone,¹⁴ dithiolene,^{15, 16} and iminotriphenylene,¹⁷ has emerged recently to combine advantages of both inorganic and organic materials. These MOFs exhibit high electrical conductivity due to full charge delocalization in the 2D plane or π - π stacking along the stacked columns.¹⁴⁻¹⁷ Interestingly, a previous theoretical investigation predicted that the 2D π -conjugated nickel-bis-dithiolene monolayer may possess a non-zero bandgap and even behave as

a topological insulator.¹⁸ Thus, these 2D MOFs could be potential candidates in the future electronics.

In this study, we select the recently synthesized semiconducting MOF, $\text{Ni}_3(2,3,6,7,10,11\text{-hexaiminotriphenylene})_2$ [$\text{Ni}_3(\text{HITP})_2$]¹⁷ as a model system. Our goal is to investigate the effect of substitution of coordinated metal ions, *e.g.* from Ni to Cu in the MOF, on the structural and electronic properties of the MOF bulks and 2D sheets. We note that these 2D $M_3(\text{HITP})_2$ sheets exhibit the Kagome-lattice pattern. By changing every coordinated metal site, the metal coordination ($dsp^2 \rightarrow sp^3$ hybridization), the geometry of in-plane network (planar \rightarrow buckled), and the electronic properties (semiconducting \rightarrow metallic) of 2D $M_3(\text{HITP})_2$ sheets are modified as shown in Fig. 1. Our theoretical work suggests high tunability of 2D MOFs with exotic electronic properties by metal substitution.

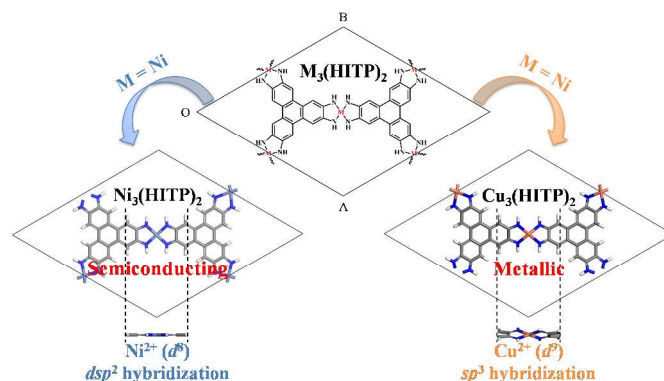


Figure 1. Illustration of 2D MOFs $M_3(\text{HITP})_2$ ($M = \text{Ni}$ and Cu). By substituting Ni with Cu, the coordination of metal site, geometry within the 2D conjugated plane, and electronic properties of the $M_3(\text{HITP})_2$ sheets are notably modified.

Computational Details

Density functional theory (DFT) methods implemented in the Vienna *ab Initio* Simulation Package (VASP 5.3.5)^{19,20} are used to optimize the three-dimensional (3D) $M_3(\text{HITP})_2$ ($M = \text{Ni}$ and Cu) bulks and 2D sheets. Before the DFT optimization for the periodic systems, the molecular units of $M_3(\text{HITP})_2$ (see Electronic Supplementary Information[†] (ESI) Fig. S1) are initially optimized at the level of B3LYP/6-31G(d), implemented in Gaussian 09 Software package.²¹ The natural-bond-orbital (NBO) analysis²² at the same level is also employed to gain insight into the coordination of $M_3(\text{HITP})_2$ later. Based on the optimized molecular units, the periodic 3D bulks and 2D sheets are then constructed. For the initial lattice constants of 3D bulk $M_3(\text{HITP})_2$ ($M = \text{Ni}$ and Cu), we refer to the predicted $\text{Ni}_3(\text{HITP})_2$ crystal structure in the previous work.¹⁷ We set the unit cell parameters $c = 6.6 \text{ \AA}$, $\alpha = \beta = 90^\circ$, and $\gamma = 60^\circ$, and then place the second $M_3(\text{HITP})_2$ layer on top of the first layer but with a parallel shift relative to the first layer by 1.8 \AA along a axis, b axis, or both a and b axes, respectively, to generate three possible crystalline structures (see ESI Fig. S2). For optimization of the 2D $M_3(\text{HITP})_2$ sheet a vacuum layer of 30 \AA is added so that the interlayer interactions are negligible. Note that for possible stacking arrangements of $M_3(\text{HITP})_2$ layers, here we only consider the above three configurations since comprehensive experimental/theoretical analysis from the powder X-ray diffraction (PXRD) and Ni K-edge extended X-ray absorption fine structure (EXAFS) measurements of $\text{Ni}_3(\text{HITP})_2$ crystal combined with DFT calculations of the potential energy surface generated by different translations between two $\text{Ni}_3(\text{HITP})_2$ layers have already been reported.¹⁷ More specifically, by comparing simulated PXRD patterns of several possible stacking arrangements with the experimental PXRD pattern, Sheberla *et al.* ruled out the staggered configuration.¹⁷ From additional EXAFS analysis, they found that the $\text{Ni}_3(\text{HITP})_2$ crystal should exhibit slipped-parallel orientation rather than the eclipsed orientation.¹⁷ Finally, with the help of DFT calculations of 82 crystals with different ab -plane displacements and a fixed interlayer separation along c , they showed that the fully eclipsed structure was energetically unfavorable and the slipped-parallel orientation wherein one $\text{Ni}_3(\text{HITP})_2$ layer was slipped relative to a neighboring layer by about 1.8 \AA along the a or b vectors gave the lowest energy on the PES.¹⁷

For computation of electronic properties (including band structures, density of states (DOS), and charge density distribution), the Perdew-Burke-Ernzerhof (PBE)²³ form for the exchange-correlation functional within the framework of the generalized gradient approximation (GGA) is employed. The Grimme's correction (D3)²⁴ is also adopted to account for weak van der Waals interactions within the organic materials. The electron-ion interaction is described by the projector augmented wave (PAW) potentials^{25,26} with an energy cutoff of 500 eV . For geometry optimization, the total energy change is set to be less than 10^{-5} eV and the magnitude of the largest force acting on the atoms is set to be less than 0.02 eV/\AA . The Brillouin zones are sampled using a $2 \times 2 \times 6$ or $4 \times 4 \times 1$ k-point mesh in the Monkhorst-Pack scheme for 3D bulks or 2D sheets, respectively.²⁷ For more accurate calculation of electronic

properties of $M_3(\text{HITP})_2$ bulks or sheets, a twice denser k-point mesh is used, and the convergence criterion of self-consistent field (SCF) computation are set to 10^{-6} eV . For the $M_3(\text{HITP})_2$ 3D bulks and 2D sheets, the spin-polarized computation is also performed to examine their magnetic properties. In addition, the effects of spin-orbit coupling (SOC) are considered to examine possible non-collinear magnetic states of the $\text{Cu}_3(\text{HITP})_2$ sheet, as well as to estimate the opening of a small bandgap in the Kagome bands of the 2D $M_3(\text{HITP})_2$ sheets.

We also examined thermal stability of both 2D $M_3(\text{HITP})_2$ sheets using *ab initio* molecular dynamics (AIMD) simulations at elevated temperatures. The AIMD simulations are performed using the QUICKSTEP program implemented in the CP2K software package.²⁸ Within the framework of the Kohn-Sham formulation of DFT and the Gaussian plane-wave (GPW) method,²⁹ the core electrons are described by the Goedecker-Teter-Hutter (GTH) normconserving pseudopotential,^{30,31} and the wave functions of valence electrons are expressed by the combination of the polarized double- ζ quality Gaussian basis³² and a plane-wave basis set (with an energy cutoff of 330 Ry). The dispersion-corrected PBE-D3 method is selected. For the $\text{Cu}_3(\text{HITP})_2$ sheet, the spin-polarized computation is applied. The AIMD simulations are performed in the constant-volume and constant-temperature ensemble with the temperature controlled at 500 K and 1000 K , respectively for each sheet. For each temperature, ten ps simulation is carried out with the time step of 1.0 fs .

Results and Discussion

3D Metallic $M_3(\text{HITP})_2$ Bulks

The previous experimental study showed that the $\text{Ni}_3(\text{HITP})_2$ crystal favored the slipped-parallel orientation between neighboring $\text{Ni}_3(\text{HITP})_2$ layers.¹⁷ In the same work, the computational study (based on PBE-D2 functional) also suggested that the 3D structure of $\text{Ni}_3(\text{HITP})_2$ in which one layer was shifted laterally with respect to the neighboring layer by about 1.8 \AA along the a axis, or b axis, or both ab axes has the lowest energy.¹⁷ Here, our DFT geometry optimization of both 3D $\text{Ni}_3(\text{HITP})_2$ and $\text{Cu}_3(\text{HITP})_2$ bulks indicates that the shift of the second layer in the unit cell along the b axis gives rise to the lowest-energy structure among the three possible crystal structures (see ESI Fig. S2). Based on the lowest-energy crystal structures, the computed electronic band structures, DOS, and the charge density isosurface for the bands crossing the Fermi level are presented in Fig. 2. As shown in Fig. 2a and 2c, both 3D $\text{Ni}_3(\text{HITP})_2$ and $\text{Cu}_3(\text{HITP})_2$ crystals are metallic with a band crossing the Fermi level along M ($1/2, 0, 0$)-L ($1/2, 0, 1/2$) and H ($2/3, 1/3, 1/2$)-K ($2/3, 1/3, 0$). The predicted metallic property of $\text{Ni}_3(\text{HITP})_2$ is consistent with the excellent bulk and thin film conductivity of 2 and $40 \text{ S}\cdot\text{cm}^{-1}$ from the two-probe and van der Pauw electrical measurements, respectively.¹⁷ Moreover, the band structures exhibit relatively strong dispersions within M-L or H-K region (see Fig. 2a and 2c), indicating strong π - π interaction between metal-organic sheets along their stacking direction (c axis). We also plot the charge density isosurface of the bands crossing the Fermi level for the $M_3(\text{HITP})_2$ bulks in Fig. 2b and 2d. These bands are mainly contributed from the out-of-plane Ni- d , C- p , and N- p delocalized states (no contribution from H atoms), consistent with interlayer metal-metal and π - π interactions. Indeed, according to the cell parameters of $M_3(\text{HITP})_2$ bulks (ESI Fig. S2), the interlayer distance between two $M_3(\text{HITP})_2$ sheets is about 3.3 \AA , which is within the van der Waals interaction

distance of 2D conjugated carbon layers, and the closest Ni···Ni and Cu···Cu distances between two sheets are 3.809 Å and 3.952 Å, respectively, indicating strong π - π interaction and weak metal-metal (d - d) interaction between the two sheets.

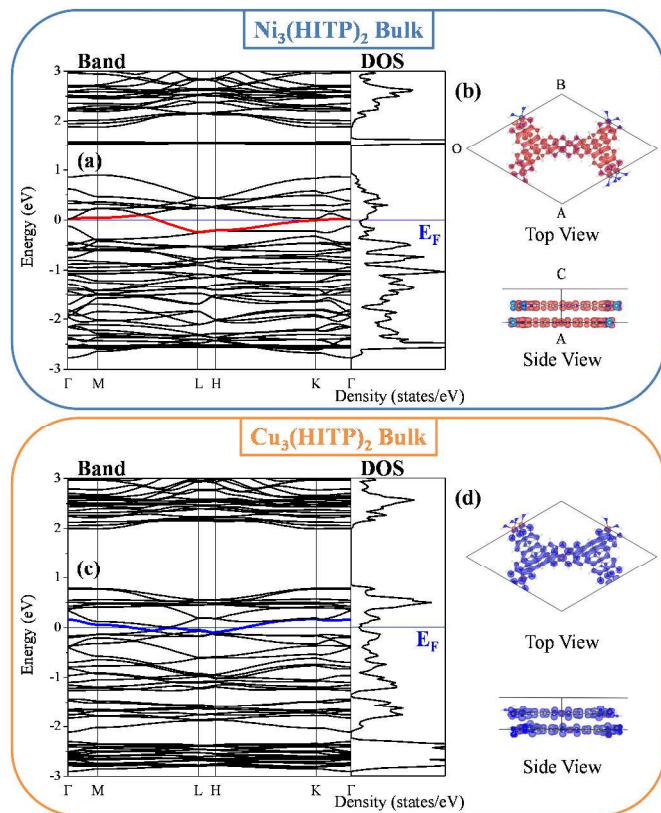


Figure 2. Computed band structures, DOS (a and c) and charge-density isosurface of bands crossing the Fermi level (b and d) of 3D $M_3(\text{HITP})_2$ ($M = \text{Ni}$ and Cu) bulks, based on the spin-nonpolarized PBE-D3 calculations. The Fermi level is marked by a thin blue line. The bands crossing the Fermi level for $\text{Ni}_3(\text{HITP})_2$ and $\text{Cu}_3(\text{HITP})_2$ are highlighted in red and blue lines, respectively. The value for charge density isosurface is $0.005 \text{ e}/\text{Bohr}^3$.

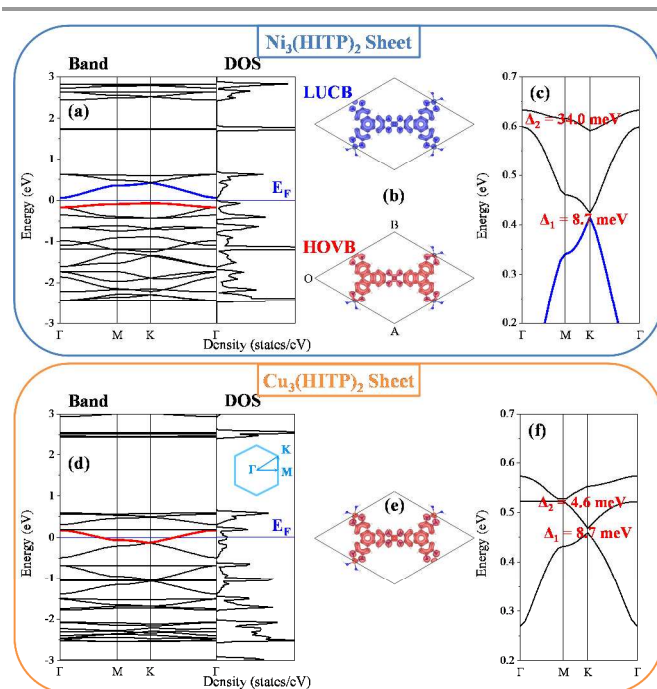


Figure 3. Computed band structures, DOS (a and d) and charge-density isosurface (b and e) from the spin-nonpolarized PBE-D3 calculation, and zoom-in Kagome bands with SOC gaps, Δ_1 and Δ_2 , (c and f) from the SOC calculations of 2D $M_3(\text{HITP})_2$ ($M = \text{Ni}$ and Cu) sheets. The Fermi level is marked by a thin blue line. The HOVB and LUCB of the $\text{Ni}_3(\text{HITP})_2$ sheet and the band crossing the Fermi level of $\text{Cu}_3(\text{HITP})_2$ sheet are highlighted in red or blue lines, respectively. The isosurface value for charge density is $0.005 \text{ e}/\text{Bohr}^3$.

2D Semiconducting $\text{Ni}_3(\text{HITP})_2$ Sheet versus Metallic $\text{Cu}_3(\text{HITP})_2$ Sheet

The reduced dimensionality from 3D $M_3(\text{HITP})_2$ bulks to 2D sheets leads to a significant change in the electronic properties. As shown in Fig. 3a and 3d, the $\text{Ni}_3(\text{HITP})_2$ sheet is a semiconductor with a small bandgap of 0.13 eV, while the $\text{Cu}_3(\text{HITP})_2$ sheet is still metallic. For the $\text{Ni}_3(\text{HITP})_2$ sheet (Fig. 3a), its valance band maximum (VBM) is located at the K point while its conduction band minimum (CBM) is located at the Γ point, suggesting $\text{Ni}_3(\text{HITP})_2$ is an indirect semiconductor. The direct bandgap at the Γ point is about 0.23 eV, slightly larger than the indirect bandgap. Since the Kohn-Sham bandgaps generally underestimate the physical bandgaps, the HSE06 functional³³⁻³⁵ is also employed to compute the band structures of the $\text{Ni}_3(\text{HITP})_2$ sheet. As shown in ESI Fig. S3, the occupied valence bands computed from the HSE06 functional exhibit a downward shift while the unoccupied conduction bands show an upward shift, compared to the PBE-D3 bands. The shift of the VBM and CBM is quite small, and the HSE06 functional results in an indirect bandgap of 0.20 eV and a direct bandgap of 0.19 eV at the Γ point, close to the PBE-D3 bandgaps. As indicated by the charge-density isosurface of the highest occupied valence band (HOVB) and of the lowest unoccupied conduction band (LUCB) for the $\text{Ni}_3(\text{HITP})_2$ sheet in Fig. 3b and of the band crossing the Fermi level for the $\text{Cu}_3(\text{HITP})_2$ sheet in Fig. 3e, these bands stem mainly from the M - d , C - p , and N - p states (no contribution from H atoms). Furthermore, the projected density of states (PDOS) of these bands (ESI Fig. S4) show that both 2D MOFs exhibit typical π -conjugated characteristics, since their PDOS near the Fermi level are almost fully contributed by the p_z orbitals of C and N

atoms as well as the delocalized d orbitals of metal atoms. For the delocalized d orbitals, only the d_{yz} and d_{xz} orbitals of Ni atoms provide contribution to both the HOVB and LUCB. In addition, the contributions of d_{yz} and d_{xz} to the HOVB or LUCB of $\text{Ni}_3(\text{HTIP})_2$ sheet are nearly the same as one another. For the $\text{Cu}_3(\text{HTIP})_2$ sheet, the four d orbitals of Cu atoms do contribute to the band crossing the Fermi level except d_{z^2} . Furthermore, from the NBO analysis, we know that the Ni atoms in the $\text{Ni}_3(\text{HTIP})_2$ sheet adopt the dsp^2 hybridization to form the square-planar geometry with the organic moieties. The $\text{Ni}_3(\text{HTIP})_2$ sheet has a perfectly 2D conjugated plane, and its HOVB and LUCB show π -bonding and π -antibonding characteristics, respectively. On the other hand, each Cu atom adopts the sp^3 hybridization. The coordination geometry of Cu atoms in the $\text{Cu}_3(\text{HTIP})_2$ sheet is slightly distorted, and thus the 2D sheet is slightly buckled.

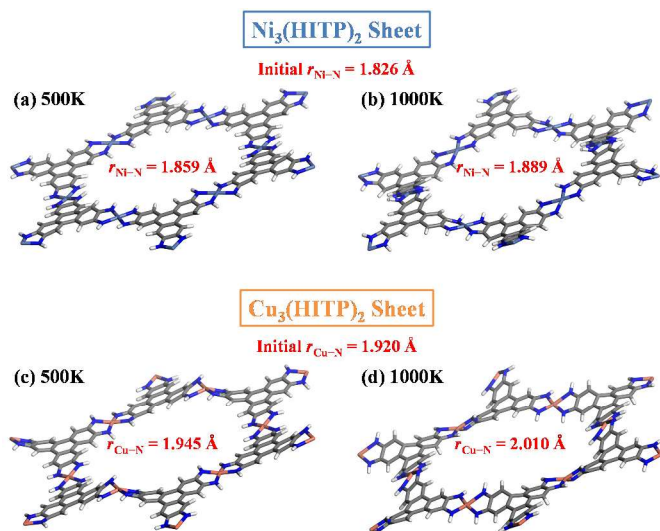


Figure 4. Snapshots of 2D $\text{M}_3(\text{HTIP})_2$ ($\text{M} = \text{Ni}$ and Cu) sheets at 500 K and 1000 K after 10 ps AIMD simulations. $r_{\text{M-N}}$ ($\text{M} = \text{Ni}$ and Cu) indicates the average bond length, and the initial $r_{\text{M-N}}$ is taken from optimized configurations.

A previous tight-binding model predicted that typical Kagome bands consist of one flat band above two Dirac bands.³⁶ The 2D metal-organic nickel-bis-dithiolene ($\text{Ni}_3\text{C}_{12}\text{S}_{12}$) lattice also exhibits similar Kagome bands with three spin degenerated bands above the Fermi level.¹⁸ The bandgap of the Dirac bands is about 13.6 meV (Δ_1), while the bandgap between the flat band and the top branch of the Dirac bands is about 5.8 meV (Δ_2).¹⁸ Moreover, the $\text{Ni}_3\text{C}_{12}\text{S}_{12}$ Kagome lattice was predicted to be a 2D organic topological insulator due to the intrinsic spin-orbit coupling of Ni ions.¹⁸ Compared to the $\text{Ni}_3\text{C}_{12}\text{S}_{12}$ Kagome lattice, the $\text{Ni}_3(\text{HTIP})_2$ sheet has different aromatic organic moieties from dithiolene to iminotriphenylene with larger conjugated C core and different coordinated organic sites from S atom to NH group. As shown in Fig. 3c, the $\text{Ni}_3(\text{HTIP})_2$ sheet has similar Kagome bands above the Fermi level as $\text{Ni}_3\text{C}_{12}\text{S}_{12}$. The higher flat band meets the top branch of the Dirac bands at the Γ point with the SOC gap (Δ_2) of 34.0 meV. The bandgap of Dirac bands is 8.7 meV (Δ_1). With substitution of the metal sites, the band structures of $\text{Cu}_3(\text{HTIP})_2$ sheet near the Fermi level become quite different from those of $\text{Ni}_3(\text{HTIP})_2$ (see Fig. 3d). As shown in Fig. 3f, the $\text{Cu}_3(\text{HTIP})_2$ sheet still has three degenerate Kagome bands and the same Dirac bandgap (Δ_1) as $\text{Ni}_3(\text{HTIP})_2$. Differently, the higher flat band meets the top branch of the Dirac bands at the

M point with a quite small SOC gap ($\Delta_2 = 4.6$ meV). Similar to $\text{Ni}_3\text{C}_{12}\text{S}_{12}$, the Fermi level of the $\text{M}_3(\text{HTIP})_2$ sheets is not located in the SOC gap. Hence, doping two (or four) electrons per unit cell in the $\text{M}_3(\text{HTIP})_2$ sheet is needed. For $\text{Ni}_3\text{C}_{12}\text{S}_{12}$, the doping concentration was predicted to be about $2 \times 10^{14} \text{ cm}^{-2}$.¹⁸ The $\text{M}_3(\text{HTIP})_2$ sheets have a longer lattice constant (about 22 Å) than the lattice constant of $\text{Ni}_3\text{C}_{12}\text{S}_{12}$ (about 15 Å). So less doping concentration, estimated to be about $8 \times 10^{13} \text{ cm}^{-2}$, is needed for the $\text{M}_3(\text{HTIP})_2$ sheets. For real device application, the electrostatic gating is required to achieve the doping effect.

Lastly, our AIMD simulations show that both 2D metal-organic Kagome lattices exhibit quite high thermal stability. Snapshots of $\text{M}_3(\text{HTIP})_2$ sheets at 500 K and 1000 K after 10 ps AIMD simulations are shown in Fig. 4. Clearly, the overall framework of both 2D MOFs become more flexible as the temperature increases. Moreover, compared to the initial average coordinated M-N ($\text{M} = \text{Ni}$ or Cu) bond lengths, both Ni-N and Cu-N bonds become longer as the temperature increases. The change of Cu-N bonds is slightly larger than that of Ni-N bonds. Nevertheless, both metal-organic networks still keep their structures even at 1000 K. It appears that their thermal stability is better than 2D organic COFs because the COFs are typically stable only up to 700 K.¹²

Conclusions

The metal substitution results in interesting changes in both geometry and electronic properties of 3D $\text{M}_3(\text{HTIP})_2$ bulks and 2D sheets. For $\text{Ni}_3(\text{HTIP})_2$, each Ni atom adopts the dsp^2 hybridization, leading to a perfect 2D conjugation. However, for $\text{Cu}_3(\text{HTIP})_2$, each Cu atom adopts the sp^3 hybridization to form a specific square-grid coordination geometry, leading to a distorted 2D sheet. The $\text{M}_3(\text{HTIP})_2$ bulks, assembled from $\text{M}_3(\text{HTIP})_2$ sheets via both strong π - π interaction and weak metal-metal interaction, are metallic. For 2D MOFs, the $\text{Ni}_3(\text{HTIP})_2$ sheet is a semiconductor with a narrow bandgap, while the $\text{Cu}_3(\text{HTIP})_2$ sheet is metallic. Importantly, the $\text{M}_3(\text{HTIP})_2$ sheets possess the Dirac bands near the Fermi level. Moreover, 2D MOFs show higher thermal stability than 2D COFs. As such, the $\text{M}_3(\text{HTIP})_2$ sheets can be promising 2D materials in place of pure 2D organic materials. With other metal ions or organic moieties for the 2D metal-organic Kagome lattices by design, new electronic or even exotic magnetic properties may be uncovered for future device applications.

Acknowledgements

We thank Dr. Wei Fa for valuable discussions. This work is supported by grants from the NSF (DMR-1420645) and by the University of Nebraska Holland Computing Center.

Notes and references

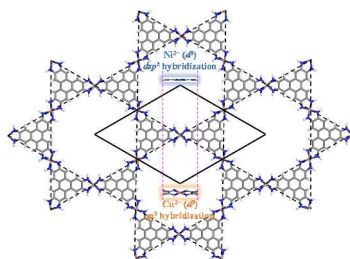
Department of Chemistry and Nebraska Center for Materials and Nanoscience, University of Nebraska-Lincoln, Lincoln, Nebraska 68588, United States

*E-mail: xzeng1@unl.edu

† Electronic Supplementary Information (ESI) available: the $\text{M}_3(\text{HTIP})_2$ building blocks, possible $\text{M}_3(\text{HTIP})_2$ crystals, HSE06 band structure and DOS of 2D $\text{Ni}_3(\text{HTIP})_2$ sheet, and PDOS of $\text{M}_3(\text{HTIP})_2$ sheets. See DOI: 10.1039/b000000x/

- 1 K. S. Novoselov, V. I. Fal'ko, L. Colombo, P. R. Gellert, M. G. Schwab and K. Kim, *Nature*, 2012, **490**, 192.
- 2 X. Huang, Z. Yin, S. Wu, X. Qi, Q. He, Q. Zhang, Q. Yan, F. Boey and H. Zhang, *Small*, 2011, **7**, 1876.
- 3 Q. H. Wang, K. Kalantar-Zadeh, A. Kis, J. N. Coleman and M. S. Strano, *Nature Nanotechnol.*, 2012, **7**, 699.
- 4 X. Feng, X. Ding and D. Jiang, *Chem. Soc. Rev.*, 2012, **41**, 6010.
- 5 S.-Y. Ding and W. Wang, *Chem. Soc. Rev.*, 2013, **42**, 548.
- 6 A. H. C. Neto, F. Guinea, N. M. R. Peres, K. S. Novoselov and A. K. Geim, *Rev. Mod. Phys.*, 2009, **81**, 109.
- 7 M. Chhowalla, H. S. Shin, G. Eda, L.-J. Li, K. P. Loh and H. Zhang, *Nature Chem.*, 2013, **5**, 263.
- 8 C. N. R. Rao, H. S. S. R. Matte and U. Maitra, *Angew. Chem. Int. Ed.*, 2013, **52**, 13162.
- 9 L. Kou, C. Tang, Y. Zhang, T. Heine, C. Chen and T. Frauenheim, *J. Phys. Chem. Lett.*, 2012, **3**, 2934.
- 10 L. Kou, T. Frauenheim and C. Chen, *J. Phys. Chem. Lett.*, 2013, **4**, 1730.
- 11 J. W. Colson and W. R. Dichtel, *Nature Chem.*, 2013, **5**, 453.
- 12 J.-J. Adjizian, P. Briddon, B. Humbert, J.-L. Duvail, P. Wagner, C. Adda and C. Ewels, *Nature Commun.*, 2014, **5**, 5842.
- 13 A. L. Elías, N. Perea-López, A. Castro-Beltrán, A. Berkdemir, R. Lv, S. Feng, A. D. Long, T. Hayashi, Y. A. Kim, M. Endo, H. R. Gutiérrez, N. R. Pradhan, L. Balicas, T. E. Mallouk, F. López-Urías, H. Terrones and M. Terrones, *ACS Nano*, 2013, **7**, 5235.
- 14 M. Hmadedh, Z. Lu, Z. Liu, F. Gándara, H. Furukawa, S. Wan, V. Augustyn, R. Chang, L. Liao, F. Zhou, E. Perre, V. Ozolins, K. Suenaga, X. Duan, B. Dunn, Y. Yamamoto, O. Terasaki and O. M. Yaghi, *Chem. Mater.*, 2012, **24**, 3511.
- 15 T. Kambe, R. Sakamoto, K. Hoshiko, K. Takada, M. Miyachi, J.-H. Ryu, S. Sasaki, J. Kim, K. Nakazato, M. Takata and H. Nishihara, *J. Am. Chem. Soc.*, 2013, **135**, 2462.
- 16 J. Cui and Z. Xu, *Chem. Commun.*, 2014, **50**, 3986.
- 17 D. Sheberla, L. Sun, M. A. Blood-Forsythe, S. Er, C. R. Wade, C. K. Brozek, A. n. Aspuru-Guzik and M. Dincă, *J. Am. Chem. Soc.*, 2014, **136**, 8859.
- 18 Z. F. Wang, N. Su and F. Liu, *Nano. Lett.*, 2013, **13**, 2842.
- 19 G. Kresse and J. Furthmüller, *Comput. Mat. Sci.*, 1996, **6**, 15.
- 20 G. Kresse and J. Furthmüller, *Phys. Rev. B*, 1996, **54**, 11169.
- 21 M. J. Frisch, G. W. Trucks and H. B. Schlegel et al, Gaussian 09, revision D.01, Gaussian, Inc., Wallingford CT, 2013.
- 22 E. D. Glendening, A. E. Reed, J. E. Carpenter and F. Weinhold, NBO, Version 3.1.
- 23 J. P. Perdew, K. Burke and M. Ernzerhof, *Phys. Rev. Lett.*, 1996, **77**, 3865.
- 24 S. Grimme, e. Antony, S. Ehrlich and H. Krieg, *J. Chem. Phys.*, 2010, **132**, 154104.
- 25 P. E. Blöchl, *Phys. Rev. B*, 1994, **50**, 17953.
- 26 G. Kresse and D. Joubert, *Phys. Rev. B*, 1999, **59**, 1758.
- 27 H. J. Monkhorst and J. D. Pack, *Phys. Rev. B*, 1976, **13**, 5188.
- 28 J. VandeVondele, M. Krack, F. Mohamed, M. Parrinello, T. Chassaing and J. Hutter, *Comput. Phys. Commun.*, 2005, **167**, 103.
- 29 G. Lippert, J. R. Hutter and M. Parrinello, *Mol. Phys.*, 1997, **92**, 477.
- 30 M. Holz, X.-a. Mao, D. Seiferling and A. Sacco, *J. Chem. Phys.*, 1996, **104**, 669.
- 31 C. Hartwigsen, S. Goedecker and J. Hutter, *Phys. Rev. B*, 1998, **58**, 3641.
- 32 J. VandeVondele and J. Hutter, *J. Chem. Phys.*, 2007, **2007**, 114105.
- 33 J. Heyd, G. E. Scuseria and M. Ernzerhof, *J. Chem. Phys.*, 2003, **118**, 8207.
- 34 J. Heyd and G. E. Scuseria, *J. Chem. Phys.*, 2004, **121**, 1187.
- 35 J. Heyd, G. E. Scuseria and M. Ernzerhof, *J. Chem. Phys.*, 2006, **124**, 219906.
- 36 E. Tang, J.-W. Mei and X.-G. Wen, *Phys. Rev. Lett.*, 2011, **106**, 236802.

Graphic Abstract



$M_3(\text{HITP})_2$ Kagome Lattice
Semiconducting $\text{Ni}_3(\text{HITP})_2$ vs Metallic $\text{Cu}_3(\text{HITP})_2$

The metal coordination, geometry of in-plane network, and electronic properties of 2D $M_3(\text{HITP})_2$ Kagome lattices are modified by metal substitution.